Biomechanics and Modeling in Mechanobiology (2021) 20:671–681
https://doi.org/10.1007/s10237-020-01409-1

ORIGINAL PAPER

Frictional performance of ostrich (*Struthio camelus*) foot sole on sand in all directions

Rui Zhang[1] · Guoyu Li[1] · Songsong Ma[1] · Hao Pang[1] · Lei Ren[1,2] · Hua Zhang[3] · Bo Su[4]

Received: 10 September 2020 / Accepted: 28 November 2020 / Published online: 22 January 2021

Abstract

To study the ostrich (*Struthio camelus*) foot sole with an irregular surface and papillae, we designed a multi-angle device to measure its friction properties on sand. The observed macro- and micro-structures of the ostrich foot sole intensified friction by tightly gripping sand particles. The sliding friction of the ostrich foot on a single-layer sand board increased with the enlarging particle size. A loose sand all-direction test showed that the coefficient of friction (COF) of the ostrich foot sole was higher than that of the nonpapillary foot. The COF of the ostrich foot sole minimized to 0.30 at 0° and maximized to 0.61 at 180°, and that of the nonpapillary foot minimized to 0.23 at 300° and maximized to 0.54 at 180°, suggesting the ostrich papillae exerted a friction effect. Significant differences in COF were observed among the ranges 10°–40°, 90° and 120°–350°, indicating the papillae can steadily enhance the frictional performance. This study provides an important theoretical basis for the design of frictional robots for deep space exploration and other soft media.

Keywords Ostrich foot sole · Plantar surface · Papillae · Macro- and micro-structures · Coefficient of friction · Frictional performance on sand

1 Introduction

The effective movement of terrestrial animals depends on the interaction between various functional parts of the body and the substrate on which they move (Dickinson et al. 2000). Since animals have evolved to adapt to the environments, the friction between feet and the substrate is related to the plantar morphology and structure (Coppack and Pulido 2004; Saalfeld and Lanctot 2017). Animal feet are functional systems that aim at either temporary or permanent attachment of an organism to the substrate surface (or to another organism) or temporary interconnection of body parts within an organism (Gorb and Beutel 2001). Animals have unique plantar morphology and structure, and their morphology depends on the evolution and particular biological function (Beutel and Gorb 2001).

At present, the detailed research on friction performance mainly focuses on the parts that contact with the medium, such as gecko feet and human fingers (Korff and McHenry 2011; Crofts and Summers 2011; Irschick and Jayne 1999). A gecko runs on smooth vertical surfaces at the speed 20 times the body length every second without falling, because its pads are covered by relatively long deformable setae that can bend and replicate the profile of the substrate (Autumn 2006; Williams and Peterson 1982). Simulation of climbing dynamics of gecko limbs based on force data showed that a small normal preload in single setae together with a 5-mm displacement led to an attachment force up to 200 mN (Autumn et al. 2001). By combining microscopic analyses

Supplementary information The online version of this article (https://doi.org/10.1007/s10237-020-01409-1) contains supplementary material, which is available to authorized users.

✉ Rui Zhang
zhangrui@jlu.edu.cn

✉ Lei Ren
lei.ren@manchester.ac.uk

1 Key Laboratory of Bionic Engineering, Ministry of Education, Jilin University, No. 5988, Renmin Street, Nanguan District, Changchun 130022, People's Republic of China

2 School of Mechanical, Aerospace and Civil Engineering, University of Manchester, Sackville Street, Manchester M13 9PL, UK

3 Aerospace System Engineering Shanghai, Shanghai, People's Republic of China

4 China North Vehicle Research Institute, Beijing 100072, People's Republic of China

and a protein assay, Derler et al. studied the friction and abrasion behaviour of the finger pad on abrasive paper and quantified skin particles abraded in friction contacts. The microscopic analyses revealed that a large number of skin particles were abraded in the form of single corneocytes, corneocyte fragments and agglomerates of corneocytes. In friction measurements, the friction coefficients of finger skins at varying normal forces were relatively high, pointing to ploughing and abrasion as important friction mechanisms (Derler et al. 2015). Meanwhile, there are many reports about the interaction between bird feet and the ground (Rubenson et al. 2004; Watson et al. 2010).

Bird feet, as typical bipeds, interact in complex ways with the substrates (Alexander 1984). The gait transitions (Daley et al. 2009; Usherwood 2010), hind limb joint angles (Reilly 2000) and obstacle-crossing posture (Birn-Jeffery et al. 2014) of birds have been studied in detail. Bird feet have advantageous functions, such as reducing energy expenditure (Zhang et al. 2017) and surmounting obstacles (Gordon et al. 2015). Gordon et al. analysed the changes in electromyographic signals of the foot and thus studied the obstacle-surmounting performance of pearl chicken moving on a treadmill. In the case of high-contrast obstacles and slower treadmill speed, changes in muscle activity were severer, which helped to improve the obstacle-surmounting performance (Gordon et al. 2015). With the help of biplanar X-rays, Falkingham reconstructed the 3D foot movements of guineafowl traversing on a granular substrate and then incorporated the kinematics into a discrete element simulation. As the soil thickness increased, footprints gradually became shallower and the force acting on sand also decreased (Falkingham and Gatesy 2014). However, there is rare quantitative research on the interaction between bird feet and granular materials.

Recent studies on the interaction between legged robots and granular materials (e.g. sand) reveal that effective locomotion on granular substrates depends on the solidification properties of the substrates (Li et al. 2009, 2011). This dependence is partially attributed to the fact that a forced granular substrate below the yield stress remains as solids, but beyond the yield stress, it flows like a fluid. Based on the solidification mechanism, we can explain and predict the rapid legged locomotion on sand by using empirical models (Li et al. 2013). For example, sea turtles, which only use solidification properties of sand under the flippers, can crawl on loose sand at a speed three times the body length per second without any slip (Mazouchova et al. 2010, 2013).

The ostrich (*Struthio camelus*) is acknowledged as the fastest and largest extant bipedal terrestrial animal with a combination of remarkable speed and exceptional endurance during locomotion on sandy environment and wasteland (Fowler 1991; Abourachid and Renous 2000; Schaller et al. 2009; Rankin et al. 2016). The ostrich can run for 30 min at 50 km/h and move at 70 km/h for short sprints. Interestingly, compared with other birds, the heavy and large ostrich has only two toes: the third major claw-bearing toe and the lateral fourth toe (Abourachid and Renous 2000; Rankin et al. 2016). Studies have described the ostrich hindlimb morphology, toe function dynamic pressure distribution and phalangeal joint kinematics during walking and running on loose sand or solid ground (Rankin et al. 2016; Rubenson et al. 2004, 2007, 2011), which underlie the research for the unique locomotor performance on a fixed or loose sand layer. Previous experiments on plantar pressure distribution of moving ostriches demonstrate that the third toe bears more of the body load than the fourth toe. As for the ground reaction force of the ostrich foot moving forwards on soft ground, the solidity of the sand beneath the toes provides sufficient traction, which may be related to the irregular surface of the foot sole (Schaller et al. 2011).

In this study, we explored the friction performance of ostrich feet with irregular plantar surface and papillae. To determine the relationship between fraction and surface roughness, we measured the friction of the ostrich foot on a single-layer sand board with different levels of roughness. To investigate the roles of the papillae and the coefficient of friction (COF) between the foot and sand at all directions, we recorded the friction of the ostrich foot with or without papillae on loose sand at 36 directions. The papillae significantly improved the frictional performance on loose sand. Scanning electron microscopy (SEM) showed that the inter-papillary gap was conductive to sand gripping.

2 Materials and methods

2.1 Ostriches

This study was approved by the Animal Experimental Ethical Inspection of Jilin University (No. 3130089). Three left ostrich feet were obtained from an ostrich farm in Ji'an, Jilin province, China. Three healthy female ostriches with height of 2.11 ± 0.01 m and weight of 68.5 ± 1.12 kg were selected. These ostriches had not been subjected to any surgical or invasive physical treatment, and had good physical conditions and appropriately elevated metatarsophalangeal joints. The three female ostriches were euthanized, and their left feet were rapidly wrapped in wet gauze to prevent water loss, and the experiments were carried out within 24 h.

2.2 Papilla morphology

The morphology of the papillae on the third and fourth toes was observed by SEM (ZEISS). An automatic stereo microscope (ZEISS SteREO Discovery V20), which

is easy-to-operate and can produce a magnification of 5–10,000 fold, was used. Typically, a dried sample was fixed on the observation table, metal-sprayed by a JFC-1600 ion sputtering device and then observed via SEM.

2.3 Custom-built friction tester

A friction tester, consisting of a multi-angle device, a fixing and loading device, a sand box [Fig. 1b (b)], a crossbeam, two displacement sensors (GEERT®, HLC-200 mm) [Fig. 1b (a)] and a force sensor (HY Chuangan, HYLY-019), was developed in-house (Fig. 1a). The force sensor had a measuring range of 0–500 N, and the displacement sensors had accuracy of 0.01 mm.

Figure 1b illustrates the multi-angle device used here, which consists of an inverted L-shaped plate (1), a roller limit plate (2), a bottom plate (3), five rollers (4), a roller end cover (5), an adjustable bearing bracket (6), a limit bearing (7), support rods (8), a sand box (14) and a displacement sensor (15). Plate (2) was fixed on plate (3) and was evenly installed with five rollers (4). Meanwhile, the axial motion of plate (3) was limited by a cover (5). Four support rods (8) were fixed vertically on plate (3) and were each installed with an adjustable bearing bracket (6). A limited bearing (7) was installed on the bearing bracket (6). When placed on a roller (4), the sand box can move along the tension direction without deflection as the bearing (7) was adjusted. Two displacement sensors (15) were fixed on plate (1), which was fixed at one end of plate (2). The sensors (15) were in close contact with the side of box (14) and can measure small displacements. To eliminate differences in displacement between the two sides of the sand box along the sliding direction, we took the mean value of the two displacement sensors as a displacement parameter.

During each experiment, an ostrich foot was fixed on the measuring device, but can move freely and be loaded in the vertical direction. The fixing and loading device consisted of an optical axis (9), a linear bearing (10), a detachable flange (12), a movable disc (13) and a fixed disc (11).

- Ostrich foot fixing method: The disc (13) with a linear bearing (10) was located on the three optical axes (9) to ensure vertical motion. The flange (12) was split into three pieces, and the ostrich foot was cement-fixed in the standing posture. The flange (12) was fixed with a nut on the movable disc (13), so the flange (12) and the ostrich foot can move vertically with the disc (13).
- Ostrich foot fixing in standing posture: A thermoplastic was completely softened in water at 80 °C and then removed to fix the foot. The thermoplastic can be softened with the temperature rise, shaped and combined with the ostrich feet in the standing posture. Then, the

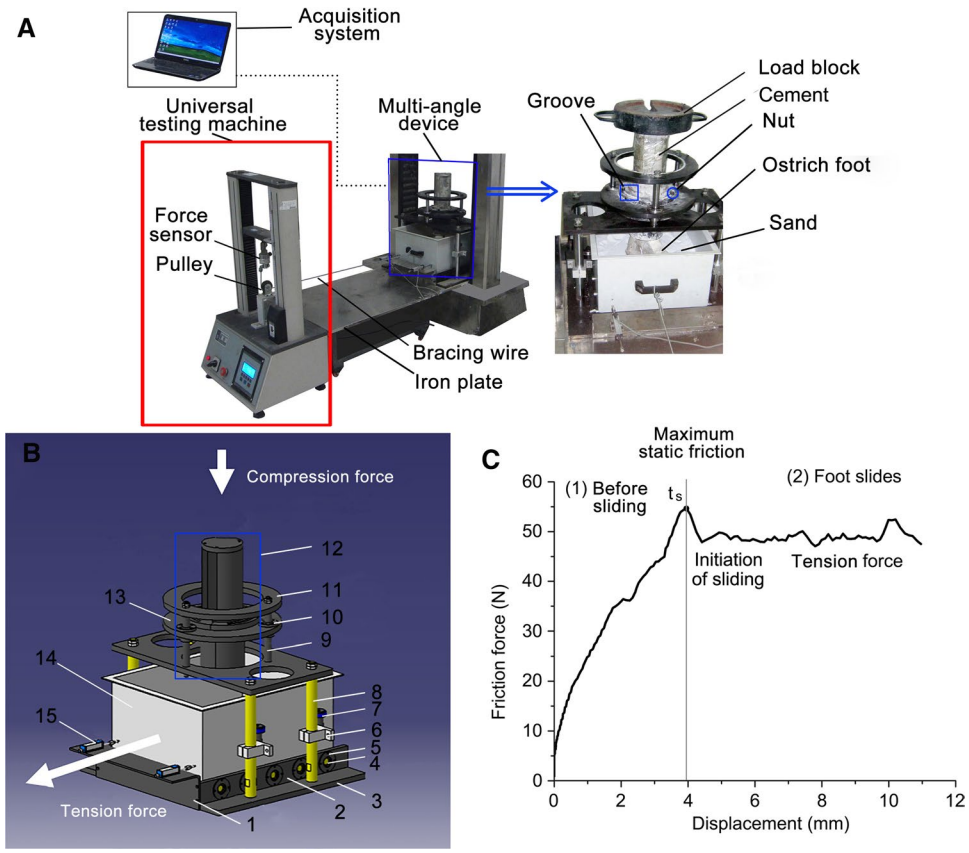

Fig. 1 Experimental tester and a sample result curve. **a** Custom-built friction tester. **b** Multi-angle device and fixing-loading device. 1: Inverted L-shaped plate; 2: roller limit plate; 3: bottom plate; 4: roller; 5: roller end cover; 6: adjustable bearing bracket; 7: limit bearing; 8: support rod; 9: optical axis; 10: linear bearing; 11: fixed disc; 12: detachable flange; 13: movable disc; 14: sand box; 15: displacement sensor. **c** Experimentally measured tension force (friction)–displacement curve for calculation of COF. The vertical load was 353.78 N, and the constant horizontal drag velocity was 60 mm/min. With increasing horizontal tension force, the friction increased until the ostrich foot began to slide horizontally (at time t_s). Afterwards, the foot slid smoothly under an applied tension force

thermoplastic was hardened after cooling and can fix the ostrich feet.

- Multi-angle measurement for ostrich feet: Numerous threaded holes existed on the detachable flange (12) as well as annular grooves on the movable disc (13). Before angle measurement, the flange (12) was nut-fixed on the disc (13) to rotate the ostrich foot (at foot axis direction) relative to the direction of sand box movement. The ostrich foot was rotated 10° per rotation, with a total of 36 rotations.

2.4 Test curves and conditions

Friction force and displacement signals were detected by the force and displacement sensors and delivered to a computer. The friction force was recorded as a function of displacement (Fig. 1c). The ostrich feet, as the only part to touch sand, need to provide all reaction forces for ostrich movement, which is similar to the adhesion of vehicle wheel surface (Zhu and Olofsson 2014). Therefore, Coulomb's law was introduced. COF was defined as the ratio of the highest point F of the curve (maximum static friction) to the normal force N of the load block (compression force perpendicular to the ostrich foot surface) of the cement-fixed ostrich foot:

$$\mu_{\mathrm{COF}} = \frac{F_{\mathrm{Friction}}(N)}{N_{\mathrm{Compression\ force}(N)}}, \tag{1}$$

- Selection of load: When a 68.5 kg ostrich was running (instant foot hitting on ground was ignored), the normal force of a single foot was around 670 N. Since a too large normal load will subject the tester to deformation, we determined a small normal load through preliminary experiments to ensure the test accuracy. Six normal loads were selected (146.00, 198.80, 265.60, 313.10, 353.78 and 373.00 N), and the average COF ($n=3$) was calculated under each load at a certain direction, where the foot axis direction was identical to the direction of foot movement. The COF was about 0.26 at the normal load of 146.00 or 198.80 N, and was about 0.30 at the normal load larger than 265.60 N (Table 1). When the normal load increased to 265.60 N, the ostrich foot was in full contact with sand and the COF was almost unchanged. Therefore, the normal load of 353.78 N was selected as the experimental load.
- Selection of velocity: A horizontal drag preliminary test with a velocity of 10–80 mm/min was carried out to determine the horizontal drag speed. When the velocity was below 50 mm/min, the acquisition curve exhibited strong fluctuations, but when it exceeded 70 mm/min, the data sampling frequency was too low, resulting in the loss of some data. The acquisition curve was stable and the sampling frequency was moderate when the velocity was 60 mm/min, which was selected as the subsequent testing velocity.

2.5 Friction measurements of ostrich feet dragging on single-layer sand boards

In the single-layer sand experiments (in which sand particles cannot move), sand particles in different sizes and 4-mm-thick boards were adhered with seccotine. Three sand boards were covered with quartz sand in three particle sizes: 0.5–1, 1–2 and 2–4 mm. The surface roughness (Ra), defined as the square root of the difference between local height and mean height (Dai et al. 2002), was determined to be 0.24, 0.52 and 1.23 mm for the three sand boards, respectively. The friction of each ostrich foot (number of measurements is $n=5$; number of ostrich feet is $N=3$) was measured in one direction, where the axis direction of the foot was identical to its moving direction.

2.6 Force measurements of ostrich feet dragging on loose sand

The friction of the tested ostrich foot ($n=5$, $N=3$) fixed to the friction tester was measured in all directions (Fig. 2). Quartz sand in particle size of 0.5–1 mm and thickness of 200 mm was selected. To ensure the quartz sand thickness was constant for each test, the same investigator used a multi-tooth harrow and a scraped board for deep loosening and scraping and conducted all tests.

2.7 Force measurements of ostrich nonpapillary feet on loose sand

The plantar papillae of two ostrich feet were removed with circlip pliers, and the friction of each foot was measured in all directions. The remaining measurements ($n=5$, $N=2$) were the same as those for the ostrich feet described above.

2.8 Statistical analyses

Two-way analysis of variance (ANOVA) was performed to analyse the differences between the ostrich foot sole and the nonpapillary foot, and the effects of orientation and foot condition (with vs. without papillae) on COF (Table 3). The significance level was set at $p<0.05$.

Table 1 Change of ostrich foot COF with normal load

Normal force	146.00	198.80	265.60	313.10	353.78	373.00
COF	0.26	0.27	0.30	0.30	0.30	0.30

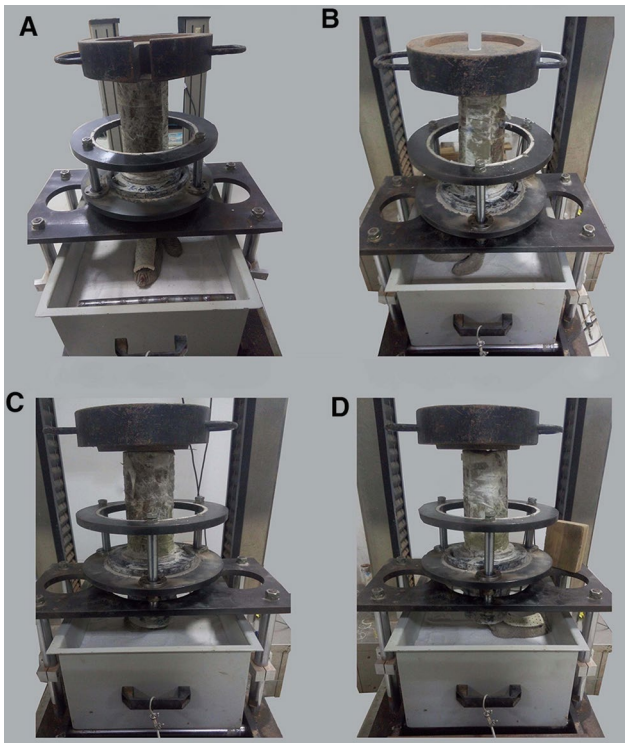

Fig. 2 Force measurements of the ostrich foot at four directions. **a** 0° (360°), **b** 90°, **c** 180° and **d** 270°

3 Results

3.1 Frictional structures of ostrich feet

The papilla bottom of the third toe is slightly frayed (Fig. 3c, d), and the papilla surface of the fourth toe is composed of transverse fine folds (Fig. 3e, f). An interpapillary gap of ~ 200 μm was found. The rough papilla surface and the bottom layer were in contact with the sand. We thought that the gap and rough papilla surface can decelerate the rolling speed of interpapillary particles and thereby tightly clamp the sand particles.

The bottom surface of the third toe is larger than that of the fourth toe, but both are irregular. The irregular surface of the third toe was divided into three parts: the smooth forepalm surface, the middle groove surface and the convex heel crown (Fig. 3b). Pits were observed on the smooth forepalm surface and the convex heel crown, which can enlarge the contact area with the sand.

The papilla structure of the third toe is gradually refined from the proximal region to the distal region, showing a columnar shape. The proximal and distal papillae of the third toe are about 1.69 and 1.39 mm in diameter, respectively. In contrast, the papillae of the fourth toe are needle-shaped, and the proximal and distal papilla are about 1.37 and 0.91 mm in diameter, respectively. Details regarding the sizes are shown in Table 2.

3.2 COF on single-layer sand boards

The COF of the ostrich foot initially increased rapidly with the increasing surface roughness (Ra) and then rose slowly (Fig. 4). As Ra increased from 0.24 to 0.52 mm and from 0.52 to 1.23 mm, the COF increased by 12.00% and 4.60%, respectively. In the single-layer sand experiments (in which sand particles cannot move), the COF relative to the foot-sand interface was measured. During the process, there was only sliding friction between the ostrich foot and the sand surface.

3.3 Difference analysis of samples on loose sand

The maximum COFs of samples A, B and C were about 0.57, 0.63 and 0.58, respectively, while the minimum values were about 0.29, 0.28 and 0.31, respectively (Fig. 5).

After the papillae were removed, only the irregular foot sole surface contacted with the sand. The maximum COFs of nonpapillary samples A_1 and B_1 were about 0.55 and 0.55, respectively, while the minimum COFs were about 0.22 and 0.24, respectively (Fig. 6). The COF of the ostrich foot sole was higher than that of the nonpapillary ostrich foot. To analyse the frictional performance of the papillae, we must exclude differences between samples.

3.4 COF for all directions on loose sand

The COF of the ostrich foot sole steadily increased by 0.31 within 0°–180°, rapidly decreased by 42.81% within 180°–260°, and then slowly dropped by 14.29% within 260°–360°. The COF of the ostrich foot sole minimized to 0.30 ± 0.028 at 0° and the maximized to 0.61 ± 0.025 at 180°. The COFs of the ostrich foot sole at 90° and 270° were 0.41 ± 0.016 and 0.33 ± 0.023, respectively.

The COF of the nonpapillary foot steadily increased by 0.26 over 0°–180°, maximizing to 0.54 ± 0.014 at 180°, and then rapidly decreased by 57.41% over 180°–300°. However, unlike the papillary foot, the COF then increased by 21.74% over 300°–360°. The COFs of the nonpapillary foot at 0°, 90° and 270° were 0.28 ± 0.0084, 0.39 ± 0.015 and 0.27 ± 0.011. The COF of the nonpapillary foot was smaller than that of the papillary foot, suggesting the papillae can enhance the frictional performance of the ostrich foot. In the loose sand experiments (in which sand particles can move), the COF relative to the foot and sand-clamped sand interface was measured. During the process, the sand particles gripped to the foot. Meanwhile, there were both sliding friction and rolling friction on the foot and sand-clamped sand interface.

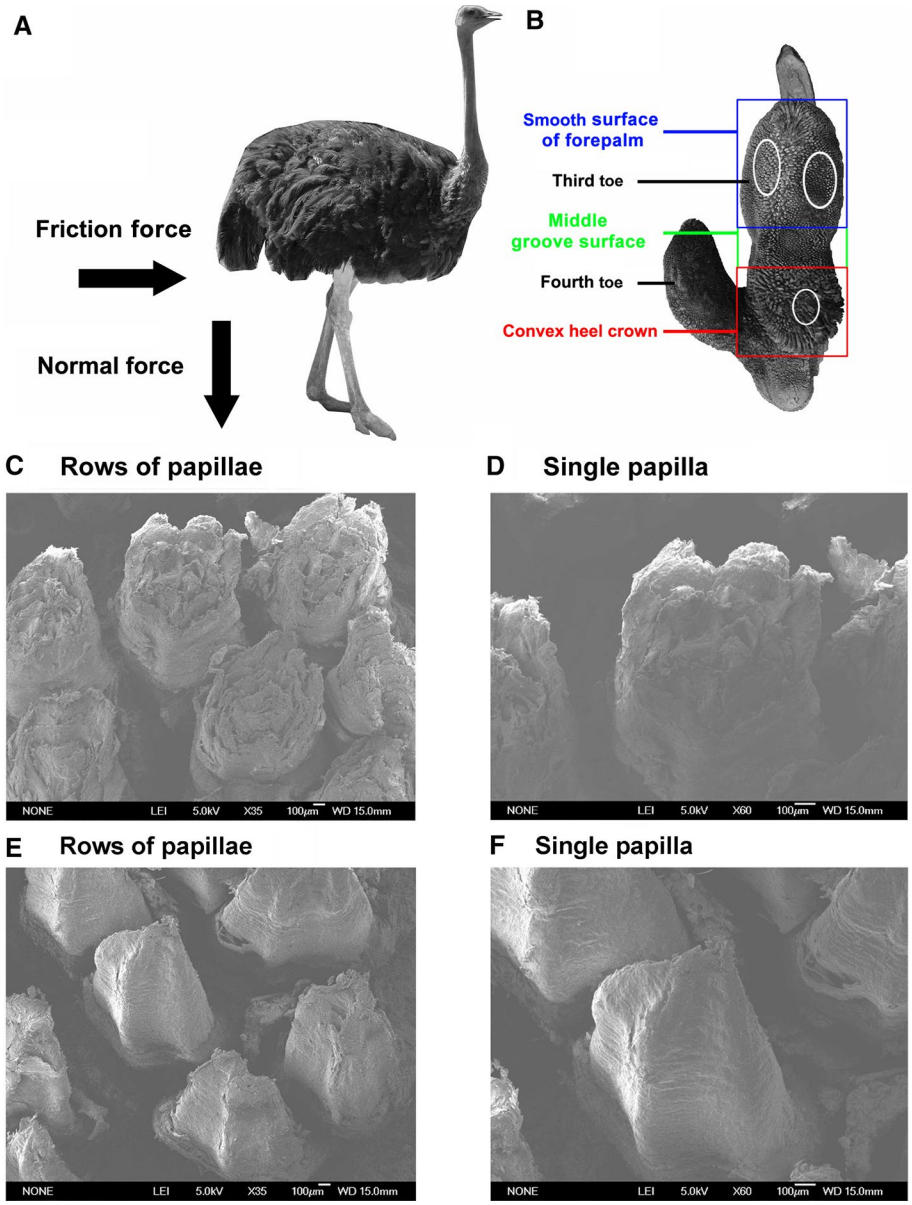

Fig. 3 Frictional structure of an ostrich foot. **a** An ostrich standing on a horizontal surface. The friction force pushes the ostrich forwards, with a compression force due to gravity. **b** Ventral view of the foot sole. The white circles indicate pits on the smooth forepalm surface and the convex heel crown. SEM images of rows of papillae from **c** the third toe and **e** the fourth toe. Single papillae of **d** the third toe and **f** the fourth toe

Table 2 Geometric dimensions of the papillae for the third and the fourth toes

Parameter	*N*	Mean (mm)	SD (mm)	Range (mm)
Third toe				
Length	30	13.07	4.40	8.42–25.60
Proximal diameter	30	1.69	0.17	1.24–1.98
Distal diameter	30	1.39	0.054	1.26–1.46
Fourth toe				
Length	30	9.13	2.36	5.48–12.44
Proximal diameter	30	1.37	0.13	1.10–1.62
Distal diameter	30	0.91	0.15	0.62–1.24

3.5 Effects of papillae on COF

No significant difference in COF was found between the ostrich foot sole and the nonpapillary foot at 50°–80°, 100°–110° or 360° (Fig. 7). Significant differences were observed in COF in the range of 10°–40°, 90° and 120°–350°, indicating the papillae can strongly enhance the frictional performance in some angle ranges. The differences of COF between the ostrich foot sole and the nonpapillary foot in the directions of 0°, 90°, 180° and 270° are 0.02, 0.03, 0.07 and 0.06, respectively. Orientation and foot condition are significant independent factors, and their interaction is significant (Table 3). Thus, the main effects of both orientation and foot condition are significant, and the combination of orientation and foot condition also affects COF.

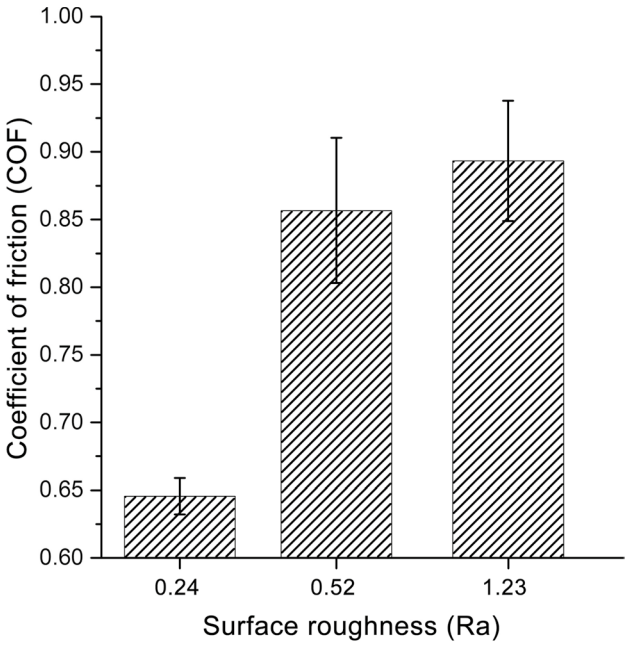

Fig. 4 COF of the ostrich foot on single-layer sand boards with different surface roughness (Ra). Error bars indicate standard deviation (SD). COF is the ratio of friction force to normal force (the same below)

4 Discussion

The macro- and micro-structures of papillae were observed, and the interpapillary gap can clamp sand particles. The pits on the smooth forepalm surface and the convex heel crown evenly contacted with the substrate, which enlarged the contact area. The ostrich foot was measured on single-layer sand boards using a custom-built friction tester, and the sliding friction of the ostrich foot increased with increasing Ra. The COF of the papillary foot was larger than that of a nonpapillary foot on loose sand, indicating the papillae can improve frictional performance.

4.1 Frictional mechanisms of irregular ostrich plantar surface and papillae

Ostriches run at high speeds on sand, and this motion is influenced by the foot structure. The motion posture of the foot is related to the running speed of ostriches (Rankin et al. 2016; Pavaux and Lignereux 1995). The contact area between the foot sole and sand is enlarged as the foot sole envelops sand particles, which contributes to an increased friction, preventing sliding (Schaller et al. 2009; Biewener and Corning 2001). We found the irregular ostrich foot surface increased the contact area, which proves the above idea. Pits observed on the smooth forepalm surface and the convex heel crown may enlarge the contact area with sand, while limiting the sand flow. When an ostrich runs on sand, the foot papillae are first expanded, which may further increase the contact area (El-Gendy et al. 2012). We found that the interpapillary gap and rough papillae surface can tightly clamp the sand particles, so as to decelerate the interpapillary particle rolling speed, which will further restrict the sand flow and increase the frictional effect. The rolling friction between the clamped sand and the papillae is

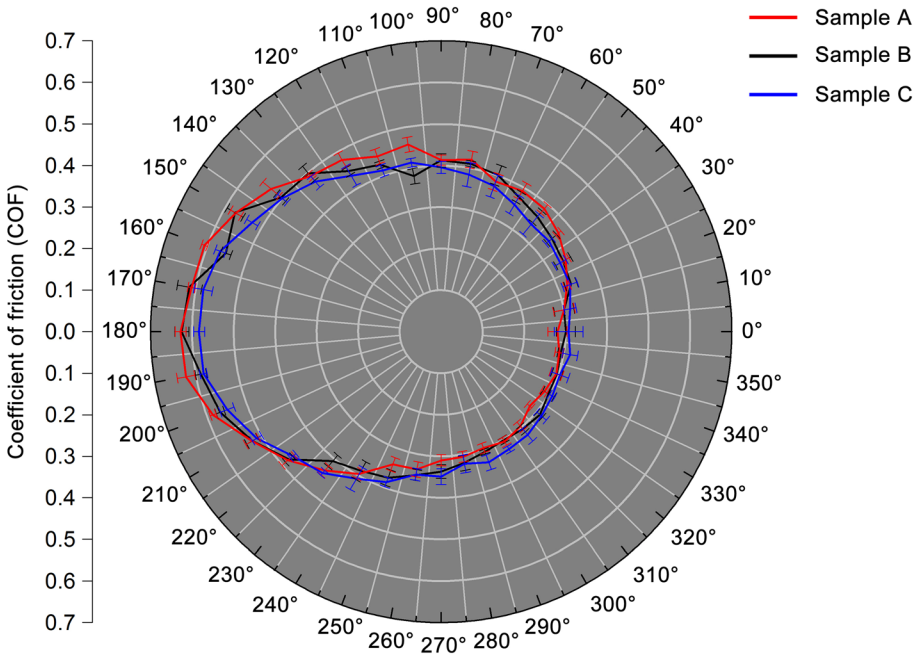

Fig. 5 COF along the 36 directions for samples A, B and C combined (mean ± SD). No significant inter-individual effects were found at $p < 0.05$

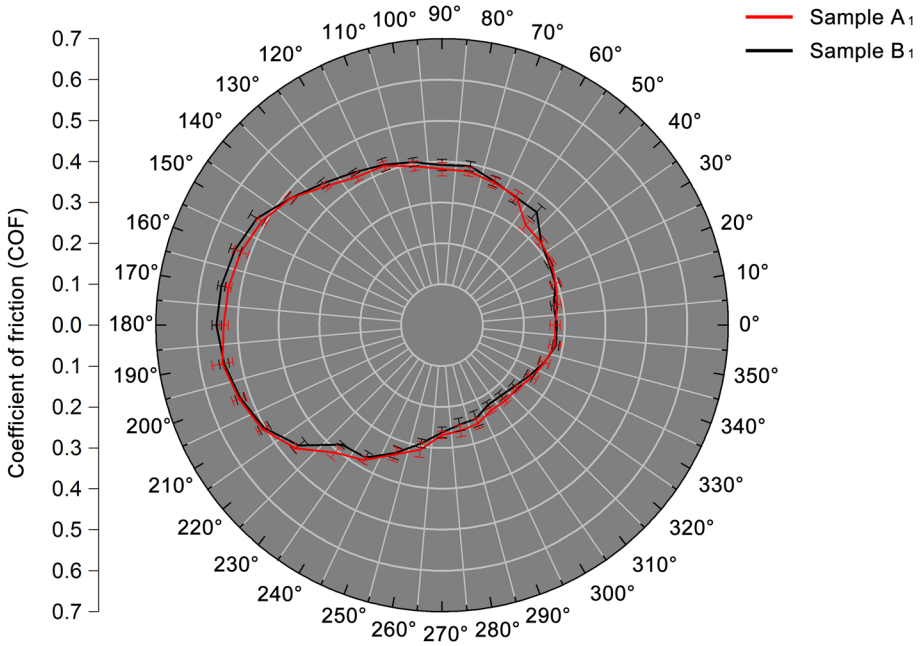

Fig. 6 COF along the 36 directions for nonpapillary samples A_1 and B_1 combined (mean ± SD). No significant inter-individual effects were found at $p < 0.05$

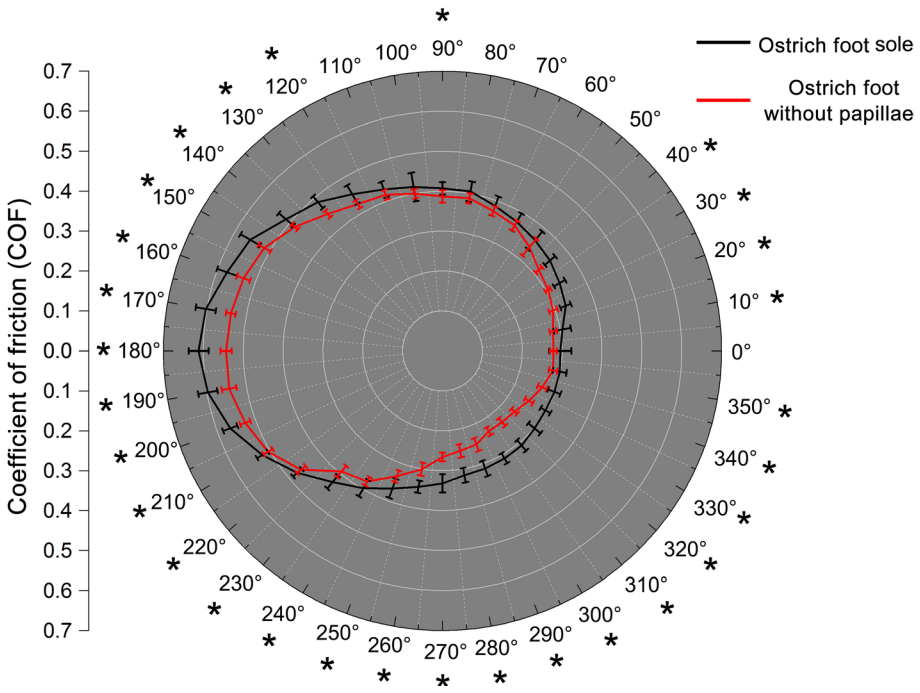

Fig. 7 Comparison of the COF and analysis of significant differences between the ostrich foot sole (black line) and the nonpapillary foot (red line). Error bars: SD; *: significant at $p < 0.05$

converted into sliding friction. Therefore, the foot condition is a significant influence factor on COF (Table 3).

The mechanism of granular material solidification was revealed by the locomotion of sea turtles on granular surfaces (Mazouchova et al. 2010). A sea turtle creates a hard sand region behind its flippers, which makes the flippers slip-less during locomotion, while the reaction force for advancing locomotion is partly supplied by the solidity of sands under the toes (Mazouchova et al. 2010). Combined with our experiments, we think the irregular surface of the ostrich foot sole may contribute to creating a hard sand region. By using high-speed videos, Li et al. obtained detailed three-dimensional running kinematics on solid and granular surfaces and revealed the locomotor mechanics of the lizard foot and the substrate. The irregular foot can produce an additional force derived, enlarging the contact surface, and solidify the sands under the foot sole (Li et al. 2012). In addition to the irregular surface of the ostrich sole, papillae were also distributed (Picasso et al. 2020). The irregular surface and the papillae of the ostrich play a

Table 3 Two-way ANOVA for orientation (36 directions) and foot condition (with vs. without papillae)

Source	Type III sum of squares	Degree of freedom (DF)	Mean square	*F* value	*P* value
Corrected model	9.53[a]	71	0.13	366.88	<0.001
Intercept	130.82	1	130.82	357,508.61	<0.001
Interaction	0.085	35	0.0020	6.62	<0.001
Orientation	8.81	35	0.25	687.71	<0.001
Foot condition	0.30	1	0.30	815.36	<0.001
Error	0.30	828	0.00		
Total	148.72	900			
Corrected total	9.84	899			

No significant differences were found among the three foot sole samples (A, B and C; all $p > 0.05$, Fig. 5) or between the two nonpapillary foot samples (A_1 and B_1; all $p > 0.05$, Fig. 6). Therefore, the data for the three ostrich foot sole samples and the data for the two nonpapillary samples were combined (Fig. 7)

[a]R Squared = 0.969 (adjusted R-squared = 0.967)

double frictional effect. Frictional performance of the ostrich during high-speed running on sandy ground is important (Zhang et al. 2017; Huang et al. 2018, 2019, 2020). We think the joint frictional system of papillae and irregular surface can improve the adaptability of ostriches to surviving on sand (Hsieh and Lauder 2004).

4.2 Relationship between papillae and ostrich locomotion and its application prospect

As we all know, efficient movement is very important for ostriches to avoid predation (John et al. 2015). How does an ostrich achieve fast motion without slipping? We think the papillae play a role. Significant differences between the ostrich foot sole and the nonpapillary foot were observed at 90°, 180° and 270° (Fig. 7), indicating the papillae play an important role in preventing ostrich feet from sliding left-, back- and rightwards. The papillae may provide friction for steering (left and right) and braking, which may be beneficial for avoiding slipping during high-speed movement. Ostriches need sufficient foot propulsion to maintain high-speed movement on sand (Watson et al. 2010). In addition, the geometrical dimensions and surface structures both influence the frictional performance (Ji et al. 2018) because the ostrich papillae directly contact with sand during movement. We found that the papillae, with rough surface structures and columnar shape, can clamp sand particles. The papillae can significantly improve the friction force and thus the movement performance of ostriches.

This study also provides a theoretical basis for the design of desert walking robots and deep space exploration. The surfaces of the Moon and Mars are both covered with loose and soft sand (Nakashima et al. 2007; Weiss and Head 2014). When a wheeled vehicle moves on the sand, it will easily sink, skid, or even be unable to drive (Hermawan et al. 2000). As the only contact part between the vehicle and the loose sand, the tire tread is essential in improving trafficability (Lang and Klüppel 2017). Based on the research on the morphology and frictional performance of irregular surface and papillae, this study theoretically underlies the research of planet rovers and anti-slip robots to improve the trafficability on loose sand.

5 Conclusions

The papillae and irregular surface of the ostrich foot sole form a joint frictional system. The irregular surface of the toes can enlarge the contact area with sand, which contributes to an increased friction. Interpapillary gaps can restrict sand flow and enhance the frictional effect. The frictional system causes the sliding friction of the ostrich foot sole to increase with surface roughness. The papillae can strongly enhance the frictional performance over some angle ranges (10°–40°, 90° and 120°–350°). And the COF at 90°, 180° and 270° can prevent the ostrich foot from sliding left-, back- and rightwards, respectively. This study provides a theoretical basis for frictional design of desert walking robots and deep space exploration.

Acknowledgements The authors are grateful for financial support by the National Natural Science Foundation of China (No. 51675221, 91748211) and the Science and Technology Development Planning Project of Jilin Province of China (No. 20180101077JC) and the Science and Technology Research Project in the 13th Five-Year Period of Education Department of Jilin Province (No. JJKH20190134KJ) and the Opening Project of the Key Laboratory of Bionic Engineering (Ministry of Education), Jilin University (No. KF20200008) and the Graduate Innovation Fund of Jilin University (No. 101832020CX156).

Author contributions The study conception was designed by Rui Zhang and Lei Ren. Material preparation, data collection and analysis were performed by Guoyu Li, Songsong Ma and Hao Pang. The first

draft of the manuscript was written by Guoyu Li. The manuscript was revised by Rui Zhang, and all authors commented on the early versions of the manuscript.

Compliance with ethical standard

Conflict of interest The authors declare no competing financial interests.

Consent for publication All authors read the manuscript and approved the publication.

References

Abourachid A, Renous S (2000) Bipedal locomotion in ratites (Paleognatiform): examples of cursorial birds. Ibis 142:538–549

Alexander RM (1984) The gaits of bipedal and quadrupedal animals. Int J Robot Res 3:49–59

Autumn K (2006) Dynamics of geckos running vertically. J Exp Biol 209:260–272

Autumn K, Liang YA, Hsieh ST, Zesch W, Chan WP, Kenny TW, Fearing R, Full RJ (2001) Adhesive force of a single gecko foothair. Nature 405:681–684

Beutel R, Gorb SN (2001) Ultrastructure of attachment specializations of hexapods (Arthropoda): evolutionary patterns inferred from a revised ordinal phylogeny. J Zool Syst Evol Res 39:177–207

Biewener AA, Corning WR (2001) Dynamics of mallard (Anas platyrynchos) gastrocnemius function during swimming versus terrestrial locomotion. J Exp Biol 204:1745–1756

Birn-Jeffery AV, Hubicki CM, Blum Y, Renjewski D, Hurst JW, Daley MA (2014) Don't break a leg: running birds from quail to ostrich prioritise leg safety and economy on uneven terrain. J Exp Biol 217:3786–3796

Coppack T, Pulido F (2004) Photoperiodic response and the adaptability of avian life cycles to environmental change. Adv Ecol Res 35:131–150

Crofts SB, Summers AP (2011) Biomechanics: swimming in the sahara. Nature 472:177–178

Dai ZD, Gorb SN, Schwarz U (2002) Roughness-dependent friction force of the tarsal claw system in the beetle pachnoda marginata (coleoptera, scarabaeidae). J Exp Biol 205:2479–2488

Daley MA, Voloshina A, Biewener AA (2009) The role of intrinsic muscle mechanics in the neuromuscular control of stable running in the guineafowl. J Physiol 587:2693–2707

Derler S, Preiswerk M, Rotaru GM, Kaiser JP, Rossi RM (2015) Friction mechanisms and abrasion of the human finger pad in contact with rough surfaces. Tribol Int 89:119–127

Dickinson MH, Farley CT, Full RJ, Koehl MAR, Kram R, Lehman S (2000) How animals move: an integrative view. Science 288:100–106

El-Gendy SA, Derbalah A, El-Magd ME (2012) Macro-microscopic study on the toepad of ostrich (Struthio camelus). Vet Res Commun 36:129–138

Falkingham PL, Gatesy SM (2014) The birth of a dinosaur footprint: subsurface 3D motion reconstruction and discrete element simulation reveal track ontogeny. Proc Natl Acad Sci U S A 111:18279–18284

Fowler ME (1991) Comparative clinical anatomy of ratites. J Zoo Wildlife Med 22:204–227

Gorb SN, Beutel RG (2001) Evolution of locomotory attachment pads of hexapods. Naturwissenschaften 88:530–534

Gordon JC, Rankin JW, Daley MA (2015) How do treadmill speed and terrain visibility influence neuromuscular control of guineafowl locomotion. J Exp Biol 218:3010–3022

Hermawan W, Yamazaki M, Oida A (2000) Theoretical analysis of soil reaction on a lug of the movable lug cage wheel. J Terramech 37:65–86

Hsieh ST, Lauder GV (2004) Running on water: three-dimensional force generation by basilisk lizards. Proc Natl Acad Sci U S A 101:16784–16788

Huang ZH, Zhang YZ, Li Q, Zhang TX, Sang N (2018) Spatially adaptive denoising for X-ray angiogram image. Biomed Signal Process Control 40:131–139

Huang ZH, Zhang YZ, Li Q, Li ZT, Zhang TX, Sang N, Xiong SQ (2019) Unidirectional variation and deep CNN denoiser priors for simultaneously destriping and denoising optical remote sensing images. Int J Remote Sens 40:5737–5748

Huang ZH, Zhang YZ, Li Q, Li X, Zhang TX, Sang N, Hong HY (2020) Joint analysis and weighted synthesis sparsity priors for simultaneous denoising and destriping optical remote sensing images. IEEE Trans Geosc. Remote Sensing 58:6958–6982

Irschick DJ, Jayne BC (1999) Comparative three-dimensional kinematics of the hindlimb for high-speed bipedal and quadrupedal locomotion of lizards. J Exp Biol 202:1047–1065

Ji AH, Zhao ZH, Manoonpong P, Wang W, Chen GM, Dai ZD (2018) A Bio-inspired climbing robot with flexible pads and claws. J Bionic Eng 15:368–378

John RH, Jeffery WR, Jonas R, Kate HR, Robert AS, Scott LD (2015) Musculoskeletal modelling of an ostrich (struthio camelus) pelvic limb: influence of limb orientation on muscular capacity during locomotion. Peerj 3:1001–1052

Korff WL, McHenry MJ (2011) Environmental differences in substrate mechanics do not affect sprinting performance in sand lizards (Uma scoparia and Callisaurus draconoides). J Exp Biol 214:122–130

Lang A, Klüppel M (2017) Influences of temperature and load on the dry friction behaviour of tire tread compounds in contact with rough granite. Wear 380:15–25

Li C, Umbanhowar PB, Komsuoglu H, Koditschek DE, Goldman DI (2009) Sensitive dependence of the motion of a legged robot on granular media. Proc Natl Acad Sci U S A 106:3029–3034

Li C, Umbanhowar PB, Komsuoglu H, Goldman DI (2011) The effect of limb kinematics on the speed of a legged robot on granular media. Exp Mech 50:1383–1393

Li C, Hsieh T, Goldman DI (2012) Multi-functional foot use during running in the zebra-tailed lizard (Callisaurus draconoides). J Exp Biol 215:3293–3308

Li C, Zhang T, Goldman DI (2013) A terradynamics of legged locomotion on granular media. Science 339:1408–1412

Mazouchova N, Gravish N, Savu A, Goldman DI (2010) Utilization of granular solidification during terrestrial locomotion of hatchling sea turtles. Biol Lett 6:398–401

Mazouchova N, Umbanhowar PB, Goldman DI (2013) Flipper-driven terrestrial locomotion of a sea turtle-inspired robot. Bioinspir Biomim 8:1748–3182

Nakashima H, Fujii H, Oida A, Momozu M, Kawase Y, Kanamori H, Aoki S, Yokoyama T (2007) Parametric analysis of lugged wheel performance for a lunar microrover by means of DEM. J Terramech 44:153–162

Pavaux C, Lignereux Y (1995) A myologic dissection of the leg and foot of the ostrich (Struthio camelus). Anat Histol Embryol 24:127–131

Picasso MBJ, Monti A, Mosto MC, Morgan CC (2020) Ontogenetic shape changes in the pelvis of the Greater Rhea (Aves, Palaeognathae) and their relationships with cursorial locomotion: a geometric morphometric approach. J Anat 00:1–9

Rankin JW, Rubenson J, Hutchinson JR (2016) Inferring muscle functional roles of the ostrich pelvic limb during walking and running using computer optimization. J R Soc Interface 13:20160035

Reilly SM (2000) Locomotion in the quail (Coturnix japonica): the kinematics of walking and increasing speed. J Morphol 243:173–185

Rubenson J, Heliams DB, Lloyd DG, Fournier PA (2004) Gait selection in the ostrich: mechanical and metabolic characteristics of walking and running with and without an aerial phase. Proc R Soc B-Biol Sci 271:1091–1099

Rubenson J, Lloyd DG, Besier TF, Heliams DB, Fournier PA (2007) Running in ostriches (Struthio camelus): three-dimensional joint axes alignment and joint kinematics. J Exp Biol 210:2548–2562

Rubenson J, Lloyd DG, Heliams DB, Besier TF, Fournier PA (2011) Adaptations for economical bipedal running: the effect of limb structure on three-dimensional joint mechanics. J R Soc Interface 8:740–755

Saalfeld ST, Lanctot RB (2017) Multispecies comparisons of adaptability to climate change: a role for life-history characteristics? Ecol Evol 7:10492–10502

Schaller NU, Herkner B, Villa R, Aerts P (2009) The intertarsal joint of the ostrich (struthio camelus): anatomical examination and function of passive structure in locomotion. J Anat 214:830–847

Schaller NU, D'Août K, Villa R, Herkner B, Aerts P (2011) Toe function and dynamic pressure distribution in ostrich locomotion. J Exp Biol 214:1123–1130

Usherwood JR (2010) Inverted pendular running: a novel gait predicted by computer optimization is found between walk and run in birds. Biol Lett 6:765–768

Watson RR, Rubenson J, Coder L, Hoyt DF, Propert MWG, Marsh RL (2010) Gait-specific energetics contributes to economical walking and running in emus and ostriches. Proc R Soc B-Biol Sci 278:2040–2046

Weiss DK, Head JW (2014) Ejecta mobility of layered ejecta craters on Mars: assessing the influence of snow and ice deposits. Icarus 233:131–146

Williams EE, Peterson JA (1982) Convergent and alternative designs in the digital adhesive pads of scincid lizards. Science 215:1509–1511

Zhang R, Han DL, Ma SS, Luo G, Li JQ (2017) Plantar pressure distribution of ostrich during locomotion on loose sand and solid ground. Peerj 5:3613–3635

Zhu Y, Olofsson U (2014) An adhesion model for wheel–rail contact at the micro level using measured 3d surfaces. Wear 314:162–170